Photoluminescence features on the Raman spectra of quasistoichiometric SiC nanoparticles: Experimental and numerical simulations

A. Kassiba,[1,*] M. Makowska-Janusik,[1,2] and J. Bouclé[1,3]
[1]*Laboratoire de Physique de l'Etat Condensé–UMR-CNRS N°6087, Faculté des Sciences, Université du Maine, Avenue O.Messiaen, 72085 Le Mans, Cedex 09, France*
[2]*Institute of Physics, Pedagogical University of Czestochowa Al.Armii Krajowej, PL42-201 Czestochowa-Poland*

J. F. Bardeau and A. Bulou
Laboratoire de Physique de l'Etat Condensé–UMR-CNRS N°6087, Faculté des Sciences, Université du Maine, Avenue O.Messiaen, 72085 Le Mans, Cedex 09, France

N. Herlin-Boime
[3]*Laboratoire Francis Perrin-SPAM-DRECAM-CEA-Saclay, 91191 Gif/Yvette-France*
(Received 24 April 2002; published 14 October 2002)

Visible photoluminescence (PL) broad bands are observed in the Raman spectra of SiC nanoparticles (np-SiC) with diameters ranging from 10 to 25 nm. The phenomenon is studied versus the particle size, chemical composition, annealing, and oxidation treatments. In the case of quasistoichiometric np-SiC, excitation by 514-nm radiation gives rise to broad red PL emissions mainly enhanced by the amorphous fraction of the particles and by the surface chemical disorder induced by oxidation. The PL spectra are quantitatively analyzed using numerical methods based on cluster approaches. PL bands are calculated as a function of the cluster geometry and defects (carbon and silicon vacancies), as well as the oxygen location within np-SiC sites. The relevance of this numerical analysis is discussed to account for the main features of the PL broad structure. The PL signature in SiC nanopowders can be used to monitor the physical organization of the np-SiC and to point out their amorphous structure fraction, surface states, and the defect contents.

DOI: 10.1103/PhysRevB.66.155317 PACS number(s): 78.67.Bf, 78.55.−m, 71.35.Cc

I. INTRODUCTION

SiC thin films are currently used in a wide range of applications such as high-power electronics and photovoltaic and optoelectronic devices.[1,2] Particularly, the search for a blue emitting device from bulk SiC was initiated two decades ago[3] and an improvement of the process was undertaken by the use of porous SiC.[4–7] In these nanoscopic or mesoscopic systems, beyond a higher photoluminescence (PL) efficiency than that in the case of bulk SiC, the PL spectra undergo large redshifts far from energies involved in interband transitions in crystalline SiC. These emissions are attributed to mechanisms mainly governed by defect states, as also shown in polycrystalline SiC or in amorphous a-SiC:H thin films giving rise to red-green luminescence at room temperature.[8] Recent works mainly focused on nanosized systems such as individual nanoobjects[9] or those created in porous matrices.[6–10] At this nanoscale, quantum confinement effects modify the electronic band structures, the vibronic states and the optical emission with respect to the bulk material.[11–13]

The present work concerns the analysis of PL broad bands superimposed to the Raman signals from SiC nanoparticles (np-SiC). The involved nanocrystallites (nc-SiC) exhibit a versatile character through the wide range of the electronic gap, modulated by crystalline polytypes, i.e., E_g (2.2 eV for $3C$-SiC and 3.33 eV for $2H$-SiC), and by the nc-SiC nanoscale size.[14] Moreover, a relaxation of chemical bonds, and the existence of defects required for the thermodynamic stability of the particle,[15,16] are expected to generate PL signals. However, instead of well-defined PL bands, only broad features are observed in the SiC nanopowders. It is therefore necessary to clarify the exact origin of the PL in np-SiC with regard to the amorphous fraction and the defects within the nanoparticles.

The second interest in these nanopowders lies in the fonctionalization of SiC-based nanocomposites such as polymer-(nc-SiC).[17] Indeed, the nanocrystalline size modulates the band energy structures and the interface states. So, when associated with suitable matrices, promising potentialities appear in nonlinear optic[17] as well as electro-optical properties which are under examination.[18] In these SiC-based composites, the interfaces play a key role in the main physical responses and the challenge lies in the control of the particle surface states. So PL studies are able to monitor the physical organization of the nanoparticles including structural features, surface states, and the involved defects. In this context, nc-SiC, with sizes ranging from 10 to 25 nm are investigated. The synthesis method is based on the CO_2 laser pyrolysis of gaseous silane and acetylene reactants.[19] The crystalline structure, composition, and np-SiC sizes can be modulated in a large extent by using appropriate reactant fluxes and laser power as well as post thermoannealing under argon or oxygen. The spectral studies are performed with confocal Raman spectrometer coupled with an argon-krypton laser for excitation. The 514-nm laser excitation is well adapted to probe the defect levels within the gap and also the emission from cubic SiC structure ($E_g = 2.2$ eV). To account for the PL phenomena quantitatively, numerical methods based on cluster approaches are developed. They consist in

the built of suitable clusters in which structural defects or vacancies can be created to fulfill geometrical optimization. Numerical simulations by quantum chemistry codes within the configuration interaction and the semiempirical parametric method (PM3) (Refs. 20–22) are undertaken. The theoretical PL bands are calculated and compared with the experimental results. These approaches allow a better understanding of the origin of the broad visible PL in np-SiC based samples.

II. EXPERIMENTAL DETAILS AND RESULTS

A. Synthesis, morphology, and structure of the nanosized SiC samples

SiC nanoparticles are synthesized by CO_2 laser pyrolysis of a gaseous mixture of silane and acetylene as reactants.[19] In the powder referred as SiC229, the reactant fluxes, which control the composition of the sample, were fixed to 150 $\mathrm{cl\,min^{-1}}$ for SiH_4 and 80 $\mathrm{cl\,min^{-1}}$ for C_2H_2 and the mixture was submitted to about 750-W laser power. The chemical analysis of the nanopowder yields an atomic ratio C/Si $=1.02\pm0.02$ which ensure that the powder is close to a stoichiometric one. TEM observations [Fig. 1(a)] evidence the homogeneous composition of the np-SiC with particle size distribution in a narrow range centered on 10 nm. High-resolution TEM images reveal that particles are composed by several crystallites, with a 2.5-nm average diameter, embedded in an amorphouslike SiC background [Fig. 1(b)]. The external particle surfaces show disordered structures probably due to a departure from the stoichiometry, as was proved in previous investigations of SiC nanopowders synthesized by the same process.[9] In order to characterize the particle size effects and their structural organization in connection with the PL signals, nanopowders with similar C/Si ratios (C/Si$=1.02\pm0.02$) and large-sized nanocrystals (25 nm) were also investigated. These samples are referred below as SiC238 and SiC241.

X-ray-diffraction (XRD) studies of the SiC229 powder give broad diffraction lines due to the low dimension of the nanocrystals and to the amorphous SiC content, in agreement with TEM observations. These broad XRD lines cannot be used to discriminate between the various SiC polytypes. More relevant structural information can be obtained from ^{29}Si magic angle spinning (MAS)-NMR measurements. Figure 2 summarizes the main features of the NMR spectra of two representative samples. The coexistence of amorphous, hexagonal and cubic SiC structures is evidenced with the corresponding relative fractions summarized in Table I. It is worth noting the overestimation of the sample amorphous fraction from NMR, mainly due to the short spin-lattice-relaxation times in amorphous structure compared to that in cubic or hexagonal lattices.

To modify the particle surface states by an elimination of residual carbon excess and surface dangling bonds, annealing treatments were performed for one hour under continuous oxygen flow at about 440, 550, and 970 °C. The carbon removal occurs by a CO_2 release and, as probed by EPR spectroscopy, the oxidation of the external particle surfaces reduces drastically the electronic defect states at the particle boundaries. IR characterizations show the appearance of Si-Si and Si-O bonds but the Si-C ones remain observed for treatment up to 970 °C (Fig. 3). Moreover, following the process described elsewhere,[9,15] other sets of thermoannealing under argon atmosphere were also performed in order to improve the crystalline order in the investigated samples.

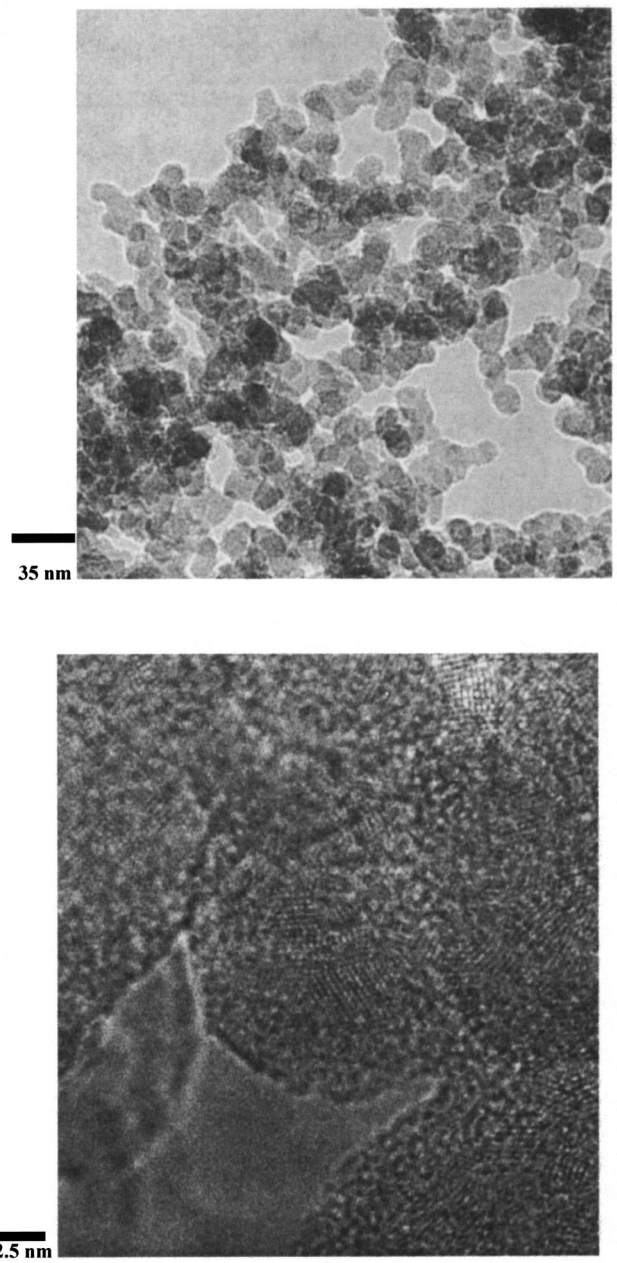

FIG. 1. TEM images of the SiC229 sample: (a) a low-resolution image evidencing the homogeneous particle diameter about 10 nm, and (b) a high-resolution image focusing on a nanoparticle composition which evidence amorphous background with nanocrystallite diameters about 2–3 nm.

B. Experimental results

Vibrational and luminescence properties are investigated by using a confocal micro-Raman spectrometer. The excita-

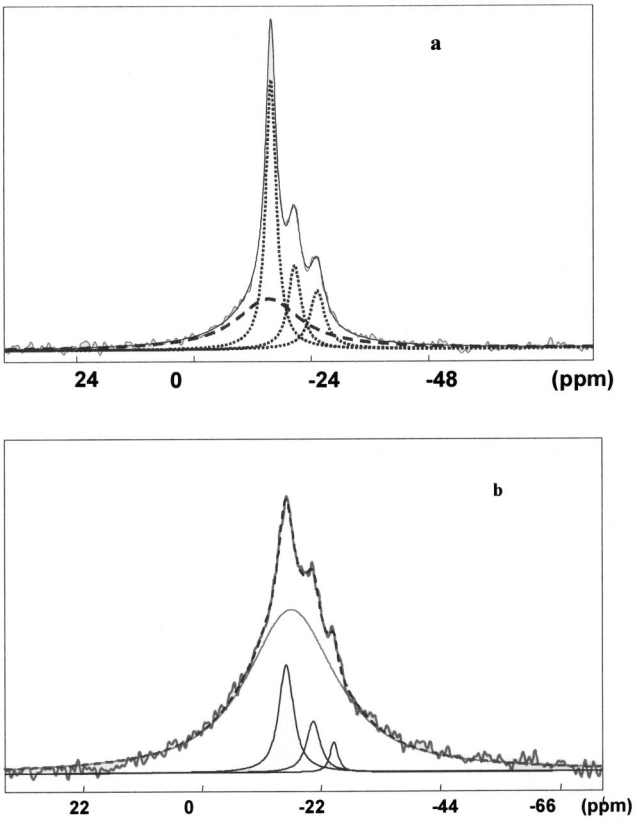

FIG. 2. ^{29}Si MAS-NMR spectra of as-formed SiC238 (a) and SiC229 (b) samples. A superposition of cubic ($3C$) and hexagonal $6H$ structures is evidenced in both samples at chemical shift (-15.61, -20.64, and -24.48 ppm). Amorphous SiC is also evidenced through the large and broad line superimposed to the structured triplet lines.

tion was realized with a 514.5-nm laser radiation of Ar^+, with 10-mW power, in order to prevent the overheating of the sample. With regard to the large spectral range on which the spectra are recorded, an appropriate calibration of the CCD detection system was realized.

Raman measurements on the as-formed batch SiC229 and oxidized ones are dominated by PL broad bands. The results reported in Fig. 4 reveal three characteristic contributions. The first is associated with vibrational properties from isolated carbon arrangements giving rise to the bands in the

TABLE I. Structural properties of SiC nanosized powders inferred from ^{29}Si MAS-NMR investigations. The rate of amorphous fraction is overestimated due to the short spin-lattice relaxation time of amorphous structure compared to that in $3C$-SiC and $6H$-SiC lattices. Also reported the paramagnetic center concentrations deduced from EPR measurements.

Sample	$6H$-SiC (%)	$3C$-SiC (%)	a-SiC (%)	Defect concentration (10^{20} cm^{-3})
SiC229	9	7	84	19
SiC241	29	26	45	6
SiC238	38	26	36	2

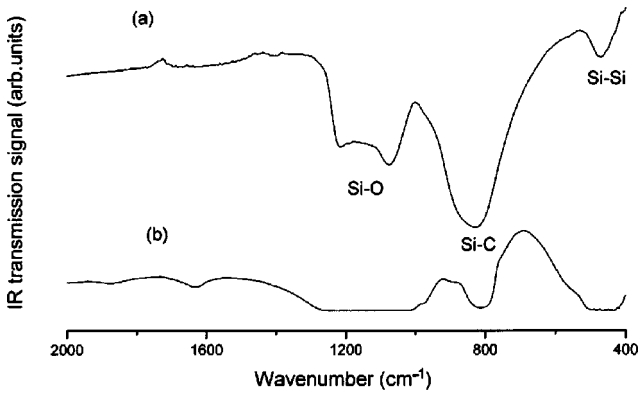

FIG. 3. IR spectra in the SiC229 sample annealed for one hour under oxygen at temperatures 440 °C (a) and 970 °C (b). It is worth noting the appearance of Si-Si and Si-O bonds with the increase of the oxidation temperature.

wavenumber range 1350–1650 cm^{-1} (inset of Fig. 4). The second contribution is from the vibrational properties of SiC (inset), which consists of a density of states with regard to the low nc-SiC size and to the high amorphous fraction in these np-SiC's. The third contribution is a broad signal in the spectral range 514–800 nm (absolute wavelength) ascribed to PL phenomena (Fig. 4). The highest PL intensity is obtained on the sample oxidized at the highest temperature.

In the SiC238 and 241 samples with large-sized nanoparticles (~25 nm), Fig. 5 point out the first- and second-order Raman lines of carbon through the resolved structures in the wave-number ranges (1350–1650 cm^{-1}; i.e., 550–575-nm absolute wavelength) and (2600–3300 cm^{-1}; i.e., 575–625 nm). The presence of the SiC structure is partly evidenced by a broad band associated with phonon density of states (inset of Fig. 4). So the vibrational properties of these nanopowders are dominated by the carbon excess mainly involved at the particle outermost surfaces and by the SiC amorphous fraction. The broad signal from PL phenomena is highly reduced

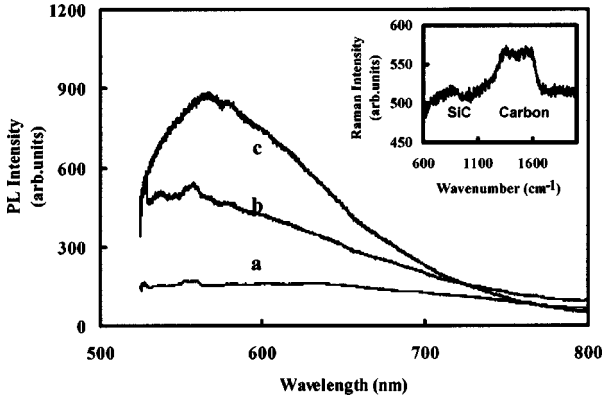

FIG. 4. Broad photoluminescence bands on the Raman spectra of SiC229 samples: (a) The as-formed sample and (b), and (c) heated samples under oxygen at temperatures 440 °C (b) and 970 °C (c). The intensities are normalized by weighting factors [1/3 (a), 1 (b), and 1/10 (c)]. In the inset we show the Raman spectrum of the as-formed SiC229 sample with vibrational bands from carbon and SiC arrangements.

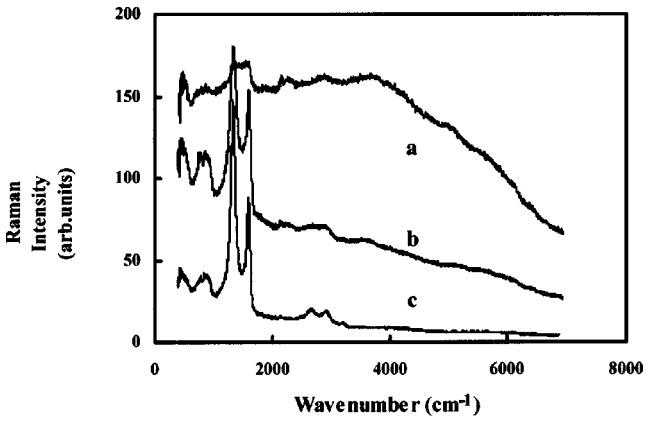

FIG. 5. Experimental Raman spectra evidencing broad PL signal from the as-formed SiC samples: (a) SiC229, (b) SiC241, and (c) SiC238. The weighting factors are [1/10 (a), 1 (b), and 1 (c)].

than in the SiC229 sample [Fig. 5(a)]. Although the SiC238 and 241 samples have similar compositions and particle sizes, their PL signals are different. As discussed below, these differences are associated with amorphous SiC and surface states. Furthermore, for the SiC238 and SiC229 samples, annealing under argon at 1200 and 1400 °C contributes to the emergence of well defined SiC Raman bands and reduction of the broad PL features (Fig. 6). Improvement of the crystalline structures and modification of the particle surfaces by a release of carbon excess are the main effects of this annealing treatment.[9]

III. NUMERICAL APPROACHES

A. Theoretical background

In order to put in light the main parameters that govern the PL response, a detailed analysis was undertaken by using numerical methods based on SiC clusters with different structures as involved in the bulk cubic ($3C$-SiC) and hexagonal ($6H$-SiC). This alternative approach, compared to *ab initio* ones, is based on semiempirical molecular methods for the treatments of the electronic interactions and vibrational states of the clusters. In the calculation of PL and vibrational properties, the cluster size is chosen such that the main features of the bulklike spectra (absorption, vibration) be correctly reproduced.[23] Clusters with 114 atoms were found relevant for this purpose. However, the central problem lies in the cluster terminating bonds. Their truncation modifies the optical band gap and alters the optical response. In our approach, terminating carbon atoms were bonded to ensure the saturation of the cluster shell. This procedure is supported by the physical organization of SiC nanoparticles probed by TEM, where the excess of carbon tends to be located at the outermost particle surface as thin layers.[9] Moreover, the convergence problem is satisfactory realized in the course of computation processes. The internal part of the clusters differs from the ideal cubic and hexagonal structure by an introduction of defects such as vacancies (Si, C) or by allowing a full geometry optimization of all the bonds giving rise to an amorphous arrangement. In this simulation part, the cluster is treated as a large molecule for which vibronic and electronic states are determined by quantum chemical codes. It is based on the self-consistent restricted and unrestricted Hartree Fock method within semi-empirical PM3 model.[21,22] A convergence is achieved when the difference between energies at iterations $(i+1)$ and (i) is less than 10^{-6} eV with typically required 500 iterations. The geometry optimization of the external carbon bonds is performed by using the molecular mechanic force field method (AMBER).[20–22]

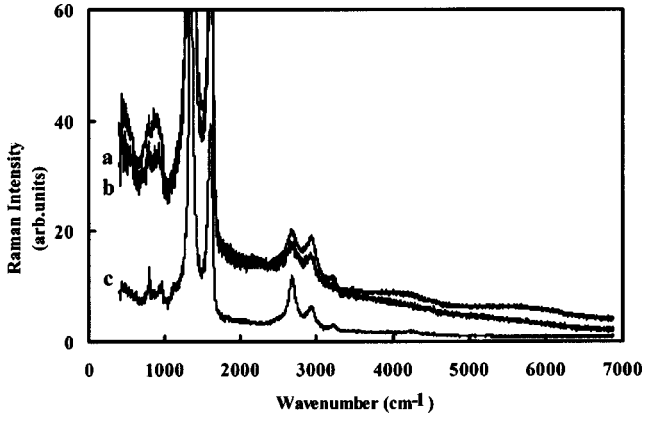

FIG. 6. Experimental Raman spectra of SiC238 sample submitted to different annealing temperatures under argon atmosphere: (a) as formed, (b) 1200 °C, and (c) 1400 °C.

For the emission process, a transition between the electronic cluster states ($|\psi_j\rangle \rightarrow |\psi_k\rangle$) gives rise to a radiation that is characterized by a single spectral line at the frequency ω_{jk}. The spectral line, per unit source volume and per solid angle unit, reads as follows:

$$I_{jk}(\omega_{jk}) \sim \frac{4\omega_{jk}^4}{3\pi^3 c^3} |(\mu)_{jk}|^2, \tag{1}$$

where $\mu_{jk} = \langle \psi_j | \nabla_r | \psi_k \rangle$ represents the dipole momentum element within the dipolar approximation, and c the light celerity. The photoluminescence spectrum is described by

$$I_{\mathrm{PL}}(\omega) \sim \sum_{j=1}^{n} \frac{(\Sigma_{i=x,y,z} |\langle \Psi_0 | \nabla_{\mathbf{r}} | \Psi_j \rangle|^2)}{(\omega - \omega_{\mathrm{ex}_j - 0})^2 + \left(\frac{\Gamma}{2}\right)^2} + \sum_{j=i,k<j}^{n} \frac{(\Sigma_{i=x,y,z} |\langle \Psi_j | \nabla_{\mathbf{r}} | \Psi_k \rangle|)}{(\omega - \omega_{\mathrm{ex}_j - \mathrm{ex}_k})^2 + \left(\frac{\Gamma}{2}\right)^2},$$

where we have taken into account the finite lifetime ($\sim 1/\Gamma$) of the emission processes with a lorentzian shape for each spectral line. $\omega_{\mathrm{ex}_j - 0}$ is the frequency difference between the exited (j) and ground (0) states while $\omega_{\mathrm{ex}_j - \mathrm{ex}_k}$ represents the frequency difference between two excited (j) and (k) states. n and ω symbols, respectively, represent the number of excited states and the excitation radiation frequency. The second sum deals with the dipolar transitions between the excited states.

According to the approach developed in molecular systems,[24] dipole momentum elements μ_{jk} were taken as differences between dipole momentum elements for j and k states as follows:

$$I_{\mathrm{PL}}(\omega)\sim\sum_{j=1}^{n}\frac{(\Sigma_{i=x,y,z}(\mu_{\mathrm{ex}_i j}-\mu_{i0})^2)}{(\omega-\omega_{\mathrm{ex}_j-0})^2+\left(\frac{\Gamma}{2}\right)^2}+\sum_{j=1,k<j}^{n}\frac{(\Sigma_{i=x,y,z}(\mu_{\mathrm{ex}_i j}-\mu_{\mathrm{ex}_i k})^2)}{(\omega-\omega_{\mathrm{ex}_j\text{-}\mathrm{ex}_i})^2+\left(\frac{\Gamma}{2}\right)^2}.$$

Such an analytical expression allows a straightforward evaluation of the PL spectra in this cluster approach. Furthermore, due to the electron-phonon interactions which contribute to the emission process by phonon-assisted transitions, the above expression is modified to take into account the vibration states. In that case, the dipole momentum matrix elements include both electronic and vibrational parts. However, with respect to the Franck-Condon rule, only the dipole momentum elements for the final transition states are affected by the vibrational contribution. In this framework, the expression

$$I_{\mathrm{PL}}(\omega)\sim\sum_{j=1}^{n}\sum_{l=1}^{m}\frac{(\Sigma_{i=x,y,z}(\mu_{\mathrm{ex}_i j}-\mu_{i0}\cdot\mu_{\Omega l})^2)}{[\omega-(\omega_{\mathrm{ex}_j-0}\pm\omega_{\Omega l})]^2+\left(\frac{\Gamma}{2}\right)^2}+\sum_{j=1,k<j}^{n}\sum_{l=1}^{m}\frac{(\Sigma_{i=x,y,z}(\mu_{\mathrm{ex}_i j}-\mu_{\mathrm{ex}_i k}\cdot\mu_{\Omega il})^2)}{[\omega-(\omega_{\mathrm{ex}_j-\mathrm{ex}_k}\pm\omega_{\Omega l})]^2+\left(\frac{\Gamma}{2}\right)^2},$$

where μ_{Ω} is the dipole momentum element for the vibrational states (l) with energies $\hbar\omega_{\Omega l}$, is used for an evaluation of the PL response from different cluster configurations.

B. Photoluminescence calculations

In a first step, the numerical procedures were performed on clusters with ideal cubic and hexagonal structures. The main goal lies in the relevance of the used approach to reproduce quantitatively the intrinsic PL spectra, which characterize the bulk SiC. Figure 7(a) shows the calculated PL bands for $3C$-SiC and $6H$-SiC clusters under an excitation line about 337 nm. The emissions bands, centered at 410 and 380 nm, correspond to pseudo-optical gaps of about 3.02 and 3.26 eV respectively. These values differ from the bulklike values 2.2 eV in $3C$-SiC and 3.0 eV in $6H$-SiC.[25] The blueshift of the calculated PL lines in $3C$-SiC compared to the bulklike gap can be accounted by the confinement effects due to the small cluster size (1.5 nm for a cluster diameter). However, in a hexagonal-like cluster, the blueshift ($\sim$200 meV) is lower than the one reported from cathodoluminescence (CL) experiments in porous p-type $6H$-SiC nanocrystallites.[26] In this case, the occurrence of a CL peak is found at 3.7 eV, i.e., a blueshift of about 700 meV. The difference is thought to be mainly accounted by the electronic active centers due to p doping. The latter are able to drastically modify the electronic structure of small nanocrystallites where quantum confinement effects occur.

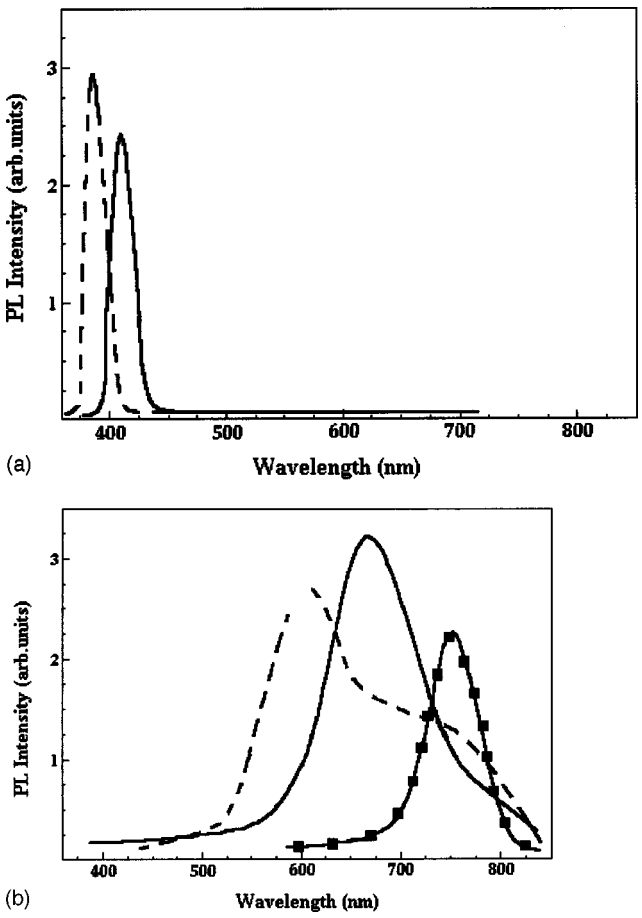

FIG. 7. (a) Theoretical PL spectra under excitation at 337 nm for crystalline SiC clusters: $3C$-SiC, full line, $6H$-SiC, dashed line. (b) Theoretical PL spectra of SiC clusters with different structures and defects: amorphous structure, full line; β-SiC; with Si-O bonds; dashed line; and a carbon cluster, line with squares. The excitation line has a wavelength in the range 460 nm$<\lambda_{\mathrm{exc}}<$520 nm.

The PL spectra calculated for an excitation radiation in the range 460 nm$<\lambda_{\mathrm{exc}}<$520 nm, for an amorphous SiC cluster, a carbon cluster, and a defected SiC cluster, by Si-O bonds, are summarized in Fig. 7(b). The last configuration reflects the oxidation effects. It is realized by SiC clusters with a fixed geometry (as in bulklike cubic or hexagonal structures) that contain (-Si-O-) bonds resulting from oxygen substitution. All the considered configurations give rise to visible photoluminescence bands centered on red wavelengths. A superposition of the theoretical spectra with appropriate weighting factors and linewidths makes it possible to explain the set of PL phenomena in the np-SiC (Figs. 4–6), as summarized below.

First, from SiC clusters with Si-O bonds, the calculated PL spectrum exhibits a main peak centered at 600 nm [Fig. 7(b)]. This account of the experimental enhancement of PL band in this spectral range with increasing oxidation temperatures (Fig. 4).

On the other hand, from the structural investigations (XRD, NMR), it was shown that amorphous SiC is involved in the np-SiC of SiC238 and SiC241 samples as well as between the nc-SiC in the SiC229 sample. The performed simulation for an amorphous cluster leads to a main contribution to the PL response by the band centered at 650 nm. The latter is smoothly resolved on the experimental spectra related to the as-formed SiC229 (Fig. 4), SiC238, and SiC241 (Figs. 5 and 6).

Finally, PL calculations for carbon clusters or for SiC clusters with Si-O bonds contribute to the PL signal in the high-wavelength range [Fig. 7(b)]. These configurations originate from the oxidized cluster and from an amorphouslike carbon cluster where both sp^2 and sp^3 bonding are involved. The latter is justified from the excess of carbon in SiC nanopowders arranged both as isolated grains and as thin turbostratic layers at the outermost particle surfaces[9] as well. The performed PL calculations account for the experimental PL signal shoulder in the spectral range around the absolute wavelength 700 nm, i.e., 6000 cm^{-1} from Figs. 5 and 6. This assignment is supported by the annealing of the SiC238 and SiC229 nanopowders at 1400 °C under argon, which favors the occurrence of a better crystalline order of SiC and the removal of carbon content. A smearing of the experimental high wavelength PL shoulder is realized both by the annealing under argon of the SiC238 [Fig. 6(c)] sample, and in the oxidized SiC229 sample [Figs. 4(b) and 4(c)] as well.

IV. DISCUSSION

The photoluminescence phenomena from SiC nanoparticles are investigated after annealing and oxidation treatments. This allows us to act on the particle structure, carbon, and defect contents. The investigated samples put in light the main role played by the different parameters on the PL responses. The oxidation effect is evidenced by the investigations of the SiC229 samples. An increase of the PL efficiency and its blueshift are induced by an increase of the oxidation temperature. Surface defect states are revealed by IR (Fig. 3) through the formation of (Si-Si) and (Si-O) bonds. The PL simulations in the SiC cluster with oxygen substitution account for the experimental results. Indeed, as shown in Fig. 7(b), the calculated PL signal is consistent with the net blue shift of the experimental PL spectrum in the oxidized sample at 970 °C. Furthermore, the creation of defected bonds with the oxidation, is not accompanied by the appearance of active electronic defects such as dangling bonds. Indeed, EPR measurements in the as-formed nanopowders show a high concentration (N_s) of unpaired electrons (Table I), which undergoes a drastic reduction with the oxidation. The possibility of fast radiative recombination of the unpaired electrons with defect states induced by oxidation can contributes to enhance the PL response. However, the decrease of the effective concentration N_s is understood only if the recombination process have characteristic times at least one order of magnitude lower than the time constant $\tau \sim 0.1$ ns of *X*-band EPR experiments. Such short recombination times are no longer involved in SiC structures.[6,27,28] So the oxidation seems to induce a curing of the electronic active defects. We emphasize that the observed visible PL in SiC nanosized powders cannot be accounted by the material defects, at least the paramagnetic ones probed by EPR.

A second parameter able to act on the PL responses is the carbon excess evidenced from the Raman signature corresponding to the sp^3 or sp^2 bonding (Figs. 4–6) in the spectral range (1350–1650 cm^{-1}). However, no correlation between the Raman intensity of the carbon bands and the PL intensity is observed. This infers that the free carbon arrangement or the carbon associated with the np-SiC did not contribute critically to the luminescence efficiency in these SiC nanopowders.

The particle size effect is analyzed through the investigated batches SiC229, SiC238, or SiC241, where the average particle diameter is 10 nm for the former sample and 25 nm for the two last samples. Although the PL phenomena in SiC229 are more important than in the samples with larger sizes, the difference cannot be attributed to size effects alone. Indeed, the samples SiC238 and SiC241, which have similar particle sizes, give rise to different PL responses. These results suggest that the main relevant parameter that monitors the visible PL comes from the fraction of amorphous structure involved in the SiC nanoparticles. The higher this fraction is (as in SiC229) the higher the PL signal is. This is evidenced by the study of SiC238 samples (Fig. 6) submitted to annealing under argon at temperature low enough to preserve the average particle size but high enough to improve the crystalline structure. Such a treatment leads to a drastic decrease of the PL intensity. We may conclude that the origin of the visible PL lies in the amorphous fraction of the SiC nanoparticles and the heterogeneous composition of the surface through the oxygen location. This later effect is thought to induce a reconstruction of SiC at the outermost particle surfaces and finally act as an amorphous structure. Indeed, a simple estimation of the pseudo-band-gap from SiC clusters with Si-O bonds gives 1.46–1.55 eV, i.e., fairly close to 1.38 eV as determined from an amorphous cluster.

V. CONCLUSION

The visible PL of SiC nanopowders is investigated versus the particle size, composition, and annealing and oxidation treatments. In these experiments, the excitation radiation (514-nm wavelength), chosen well below the SiC crystalline optical gap of hexagonal SiC, was found appropriate to point out the main relevant structural and chemical parameters of the emission phenomena. Thus the PL responses, which consist of intense red emissions, are mainly governed by the SiC amorphous fractions of nanopowders and by the occurrence of Si-O bonds consecutive to the oxidation. The developed model for PL simulations by quantum-chemical codes is based on clusters with a convenient size, different geometries and defected bonds. PL bands are calculated in different configurations including amorphous clusters and those with oxygen location in SiC sites which account for oxidation effects. The assignment of the features of these PL spectra is in agreement with the experimental structural and composition peculiarities.

ACKNOWLEDGMENTS

One of us (M.M.J.) would like to thank the Region Pays de la Loire (France) for the financial support (post-doctoral grant). We are grateful to Dr. Jean Vicens (LERMAT-Caen-France) for MET images and to Professor Joel Emery (LPEC-Le Mans) for performing the NMR spectra on SiC nanopowders. Dr. Cécile Raynaud (LFP-SPAM-Saclay) is acknowledged for a critical reading of the manuscript. We are indebted to Dr. Gilles Dujardin (LSO-Le Mans) and Dr. Fabienne Poncin-Epaillard (LCO2M-Le Mans) for the IR spectra recording.

*Corresponding author A. Kassiba. Email address: (kassiba@univ-lemans.fr) Tel. +33.2.43.83.35.12, Fax. +33.2.43.83.35.18

[1] B. Delley and E. F. Steigmeier, Phys. Rev. B **47**, 1397 (1993).
[2] L. Tsykeskov, J. V. Vandyshev, and P. M. Fauchet, Phys. Rev. B **49**, 7821 (1994).
[3] M. Ikeda, T. Hayakawa, S. Yamagiwa, H. Matsunami, and T. Tanaka, J. Appl. Phys. **50**, 8215 (1979).
[4] L. S. Liao, X. M. Bao, Z. F. Yang, and N. B. Min, Appl. Phys. Lett. **66**, 2382 (1995).
[5] S. Kim, J. Spanier, and I. P. Herman, Jpn. J. Appl. Phys. **39**, 5875 (2000).
[6] O. Jessensky, F. Muller, and U. Gosele, Thin Solid Films **297**, 224 (1997).
[7] H. Mimura, T. Matsumoto, and Y. Kanemitsu, J. Non-Cryst. Solids **198**, 2 (1996).
[8] F. Giorgis, A. Chiodoni, G. Cicero, S. Ferrero, P. Mandracci, G. Barucca, R. Reitano, and P. Musemeci, Diamond Relat. Mater. **10**, 1264 (2001).
[9] S. Charpentier, A. Kassiba, A. Bulou, M. Monthioux, and M. Cauchetier, Eur. Phys. J.: Appl. Phys. **8**, 11 (1999).
[10] I. V. Kityk, A. Kassiba, and S. Benet, J. Cluster Sci. **12**, 399 (2001).
[11] G. S. Solomon, M. Pelton, and Y. Yamamoto, Phys. Rev. Lett. **86**, 3903 (2001).
[12] Y. P. Guo, J. C. Zheng, A. T. S. Wee, C. H. A. Huan, K. Li, J. S. Pan, Z. C. Feng, and S. J. Chua, Chem. Phys. Lett. **339**, 319 (2001).
[13] Y. Glinka, S. H. Lin, L. P. Hwang, Y. T. Chen, and N. H. Tolk, Phys. Rev. B **64**, 085421 (2001).
[14] I. V. Kityk, A. Kassiba, J. Berdowski, and K. J. Plucinski, Phys. Lett. A **265**, 403 (2000).
[15] S. Charpentier, A. Kassiba, J. Emery, and M. Cauchetier, J. Phys.: Condens. Matter **11**, 4887 (1999).
[16] I. V. Kityk, A. Kassiba, K. Tuesu, S. Charpentier, Y. Ling, and M. Makowska-Janusik, Mater. Sci. Eng., B **77**, 147 (2000).
[17] I. V. Kityk, M. Makowska-Janusik, A. Kassiba, and K. J. Plucinski, Opt. Mater. **13**, 449 (2000).
[18] J. Bouclé, A. Kassiba, I. V. Kityk, M. Makowska-Janusik, S. Sanetra, N. Herlin-Boime, and M. Mayne, Phys. Lett. A (to be published).
[19] M. Cauchetier, O. Croix, and M. Luce, Adv. Ceram. Matter **3–6**, 197 (1988).
[20] HyperChem ™, Hypercube, Inc. FL.
[21] S. J. Weiner, P. A. Kollman, D. A. Case, U. C. Ghio, G. Alagona, Jr., S. Profeta, and P. Weiner, J. Am. Chem. Soc. **106**, 765 (1984).
[22] S. J. Weiner, P. A. Kollman, D. T. Nguyen, and D. A. Case, J. Comput. Chem. **7**, 230 (1986).
[23] A. Kassiba, M. Makowska-Janusik, J. Bouclé, J. F. Bardeau, A. Bulou, N. Herlin-Boime, M. Mayne, and X. Armand, Diamond Relat. Mater. **11**, 1243 (2002).
[24] J. L. Oudar and D. S. Chemla, J. Chem. Phys. **66**, 2664 (1977).
[25] Y. Park, in *SiC Materials and Devices, Semiconductors, and Semimetals* (Academic, London, 1998).
[26] J. S. Shor, L. Bemis, I. Grimberg, and B. Z. Weiss, J. Appl. Phys. **76**, 1 (1994).
[27] M. B. Yu, Rusli, S. F. Yoon, S. J. Xu, K. Chew, J. Cui, J. Ahn, and Q. Zhang, Thin Solid Films **377–378**, 177 (2000).
[28] O. Brandt, J. Ringling, K. H. Ploog, H. J. Wünsche, and F. Henneberger, Phys. Rev. B **58**, R15977 (1998).